Electronic Supplementary Information

(ESI)

Towards multifunctional lanthanide-based metal-organic frameworks

Gerard Tobin,[a] Steve S. Comby,[b] Nianyong Zhu,[a,c] Rodolphe Clérac,[d,e] Thorfinnur Gunnlaugsson,[b] and Wolfgang Schmitt [a*]

[a] School of Chemistry and Centre for Research on Adaptive Nanostructures and Nanodevices (CRANN), University of Dublin, Trinity College Dublin, Dublin 2, Ireland, E-mail: schmittw@tcd.ie; [b] School of Chemistry and Trinity Biomedical Sciences Institute, University of Dublin, Trinity College Dublin, Dublin 2, Ireland; [c] Department of Chemistry, Hong Kong Baptist University, Hong Kong, HK; [d] CNRS, CRPP, UPR 8641, F-33600 Pessac, France; [e] Univ. Bordeaux, CRPP, UPR 8641, F-33600 Pessac, France

1 Syntheses and Methods

1,3,5-Benzene-trisethynylbenzoic acid (BTEB) was synthesied following a method described by R. K. Castellano and J. Rebek, Jr., *J. Am. Chem. Soc.*, **1998**, *120*, 3657.

Synthesis of TCM-9-Ho

A solution of BTEB (0.04 g, 0.08 mmol) in DMF (5 ml) was added to a 10 ml glass vial containing holmium nitrate pentahydrate (0.009 g, 0.02 mmol). The mixture was sonicated for 10 minutes, the vial was sealed and heated for 72 hours at 100 ^{o}C. After cooling to room temperature, the resulting small, pale pink crystals of [Ho(BTEB)(H_2O)$_2$].5DMF were washed with DMF (x3) and stored in DMF. Yield: *ca.* 20%; FT-IR (diffuse reflectance) $\overline{\nu}_{max}$ cm^{-1}: 2925(br), 1670(s), 1624(s), 1604 (s), 1582 (s), 1535 (s), 1501 (m), 1407 (s), 1380 (s). 1257 (m), 1177 (w), 1090 (s), 1017 (m), 858 (m), 781 (s); Elemental analysis (%) for [Ho(BTEB)(H_2O)$_2$].5DMF: Expected: C, 53.68; H, 5.07; N, 6.52. Found: C, 52.57; H, 4.71; N, 6.94.

The related lanthanide-based MOFs prepared using analogous synthetic procedures to that used to synthesise **TCM-9-Ho**, with the relevant lanthanide nitrate replacing holmium nitrate pentahydrate at corresponding mole ratios. The obtained yields vary between 25-40%.

TCM-9-Dy: FT-IR (diffuse reflectance) $\overline{\nu}_{max}$ cm^{-1}: 1666(s), 1624 (s), 1604 (s), 1581 (s), 1535 (s), 1413 (s), 1380 (s), 1092 (s), 1017 (m), 858(m), 781 (s); Elemental analysis (%) for [Dy(BTEB)(H_2O)$_2$].5DMF, Expected: C, 53.81; H, 5.08; N, 6.54. Found: C, 52.31; H, 4.61; N, 6.81.

TCM-9-Tb: FT-IR (diffuse reflectance) $\overline{\nu}_{max}$ cm^{-1}: 1662(s), 1621 (s), 1603 (s), 1581 (s), 1534 (s), 1413 (s), 1384 (s), 1090 (s), 1017 (m), 857(m), 782 (s); Elemental analysis (%) for [Tb(BTEB)(H_2O)$_2$].5DMF, Expected: C, 53.99; H, 5.10; N, 6.56. Found: C, 52.69; H, 4.97; N, 6.75.

TCM-9-Eu: FT-IR (diffuse reflectance) $\overline{\nu}_{max}$ cm^{-1}: 1661(s), 1620 (m), 1603 (s), 1580 (s), 1534 (s), 1413 (s), 1382 (s), 1091 (s), 1017 (m), 855(m), 782 (s); Elemental analysis (%) for [Eu(BTEB)(H_2O)$_2$].5DMF, Expected: C, 54.34; H, 5.08; N, 6.54. Found: C, 53.19; H, 4.76; N, 7.02.

TCM-9-Yb: FT-IR (diffuse reflectance) $\overline{\nu}_{max}$ cm^{-1}: 1658(s), 1626 (m), 1602 (s), 1578 (s), 1531 (s), 1413 (s), 1382 (s), 1093 (s), 1017 (m), 860(m), 781 (s); Elemental analysis (%) for [Yb(BTEB)(H_2O)$_2$].5DMF, Expected: C, 53.28; H, 5.03; N, 6.47. Found: C, 52.18; H, 4.66; N, 7.19.

TCM-9-Er: FT-IR (diffuse reflectance) $\overline{\nu}_{max}$ cm^{-1}: 1654 (s), 1625 (m), 1602 (s), 1578 (s), 1528 (m), 1411(s), 1382 (s), 1094 (s), 1017 (m), 860 (m), 781 (s); Elemental analysis (%) for [Er(BTEB)(H_2O)$_2$].5DMF Expected: C, 53.57; H, 5.06; N, 6.51. Found: C, 52.01; H, 4.62; N, 6.90.

TCM-9-Nd: FT-IR (diffuse reflectance) $\bar{\nu}_{max}$ cm^{-1}: 1665 (s), 1605 (s), 1577 (s), 1517 (s), 1505 (sh), 1409 (s), 1387 (s), 1255 (w), 1174 (w), 1090 (s), 855 (m), 784 (s); Elemental analysis (%) for proposed formula of $[Nd(BTEB)(H_2O)_2].5DMF$ Expected: C, 54.74; H, 5.17; N, 6.65. Found: C, 54.64; H, 3.40; N, 3.90.

TCM-9-Sm: FT-IR (diffuse reflectance) $\bar{\nu}_{max}$ cm^{-1}: 1665 (s), 1604 (s), 1577 (s), 1522 (s), 1503 (sh), 1411 (s), 1384 (s), 1253 (w), 1177 (w), 1090 (s), 855 (m), 783 (s); Elemental analysis (%) for proposed formula of $[Sm(BTEB)(H_2O)_2].5DMF$, Expected: C, 54.42; H, 5.14; N, 6.61. Found: C, 53.89; H, 3.38; N, 3.75.

Methods:

X-ray powder diffraction: X-ray powder diffraction measurements were performed using a Siemens D500 diffractometer with a Cu-K α_1 radiation with a wavelength of $\lambda = 1.54056$ Å.

Magnetic measurements: Measurements were performed at the Centre de Recherche Paul Pascal, CNRS, France. The magnetic susceptibility measurements were obtained with the use of a MPMS-XL Quantum Design SQUID magnetometer. This magnemometer operates between 1.8 and 300 K for dc applied fields ranging between -7 to 7 T. Measurements were performed on a polycrystalline samples of 13.53 mg and 13.65 mg for **TCM-9-Ho** and **TCM-9-Dy**, respectively, which were taken from the mother liquor and immediately placed inside a polyethylene bag (3 × 0.5 × 0.02 cm) to prevent solvent loss. ac susceptibility measurements were measured with an oscillating ac field of 3 Oe with frequency between 1 to 1500 Hz. It is worth noting that no out-of-phase ac susceptibility signal has been detected above 1.8 K. The magnetic data were corrected for the sample holder and diamagnetic contributions.

Photoluminescence spectroscopy: Solid state photoluminescence spectroscopy were recorded on a Fluorolog-3 (Horiba Jobin Yvon) spectrophotometer. Spectra measured in the UV/visible range used a room temperature R9281x photomultiplier tube as the detector. Near-Infrared (NIR) spectra were measured using a liquid nitrogen cooled R5509 photomultiplier tube as the detector. Emission and excitation spectra were corrected for the wavelength response of the system and the intensity of the lamp profile over the excitation range, respectively, using correction factors supplied by the manufacturer. Photostability and lifetime measurements were conducted using a Varian-Cary-Eclipse luminescence spectrometer.

Nitrogen sorption: Measurements were performed on an Autosorb-IQ (Quantachrome) volumetric analyser. Samples were outgassed at 10^{-6} torr at the specified temperature. The dead volume was estimated using helium, under the assumption that it is not absorbed at any of the studied temperatures. Measurements undertaken at 77 K were performed in a liquid N_2 bath. To provide high accuracy and precision in determining p/p_0, the saturation pressure was measured throughout the gas sorption measurements by means of a dedicated saturation pressure transducer. Ultra-high grade N_2 (99.999% purity) was used throughout the experiments. The surface area of the relevant samples were determined from the N_2 isotherms.

2 Single Crystal X-ray Diffraction of TCM-9-Ho

Data were collected on a Bruker APEX II DUO CCD diffractometer equipped with a IμS CuK_α microfocus tube (wavelength of 1.54184 Å). The single crystals were cooled to 173(2) K, using an Oxford Cryostream low-temperature device. The diffraction frames were integrated and processed using the Bruker SAINT software package. The data were corrected for absorption effects using the multi-scan method (SADABS).[S1] The space group was determined using XPREP, and the structure was solved by direct methods (SHELXS) and extended/refined using the SHELXL program.[S2] The positional and anisotropic displacement parameters for the non-hydrogen atoms were refined. Hydrogen atoms were constrained to idealized geometries and allowed to ride on their carrier atoms with an isotropic displacement parameter related to the equivalent displacement parameter of their carrier atoms. The structure contains solvent accessible void volume in which solvent molecules could not be located reliably. To account for this, the Platon-Squeeze routine[S3] was used to calculate the void volumes and re-generate reflections files by excluding the diffraction contributions of these un-located solvent molecules. Crystal data and numerical details for the data collection and refinement are given in Table S1. Final fractional atomic coordinates, equivalent displacement parameters and anisotropic displacement parameters for the non-hydrogen atoms are given in the cif-file.

Crystallographic data, CCDC number 1405181, can be obtained free of charge from the Cambridge Crystallographic Data Centre *via* www.ccdc.cam.ac.uk/data_request/cif.

[S1] Bruker. SADABS. 2001, Bruker AXS Inc., Madison, Wisconsin, USA.
[S2] G. M. Sheldrick, *Acta Cryst.* 2008, **A64**, 112-122.
[S3] A. L. Spek, *Acta Cryst.* 2009, **D65**, 148-155.

Table 1. Crystal data and structure refinement for **TCM-9-Ho**.

Identification code	shelx	
Empirical formula	$C_{36}H_{30}HoNO_{11}$ for $[Ho(H_2O)_2(BTEB)](DMF)(H_2O)_2$	
Formula weight	817.54	
Temperature	173(2) K	
Wavelength	1.54184 Å	
Crystal system	Orthorhombic	
Space group	I m a 2	
Unit cell dimensions	a = 21.403(6) Å	α= 90°.
	b = 34.255(9) Å	β= 90°.
	c = 8.023(2) Å	γ = 90°.
Volume	5882(3) $Å^3$	
Z	4	
Density (calculated)	0.923 Mg/m^3	
Absorption coefficient	2.820 mm^{-1}	
F(000)	1632	
Crystal size	0.10 × 0.01 × 0.01 mm^3	
Theta range for data collection	2.434 to 70.073°.	
Index ranges	$-26 \le h \le 26$, $-41 \le k \le 41$, $-7 \le l \le 9$	
Reflections collected	27706	
Independent reflections	5370 [R(int) = 0.1263]	
Completeness to theta = 67.684°	98.9 %	
Absorption correction	Semi-empirical from equivalents	
Max. and min. transmission	0.7454 and 0.4845	
Refinement method	Full-matrix least-squares on F^2	
Data / restraints / parameters	5370 / 330 / 211	
Goodness-of-fit on F^2	1.507	
Final R indices [$I > 2\sigma(I)$]	R_1 = 0.1469, wR_2 = 0.3668	
R indices (all data)	R_1 = 0.2130, wR_2 = 0.4213	
Absolute structure parameter	0.54(10)	
Largest diff. peak and hole	2.909 and -3.048 e.$Å^{-3}$ (near Ho atom, others lower than 1)	

3 Powder X-ray Diffraction of TCM-9-Ho

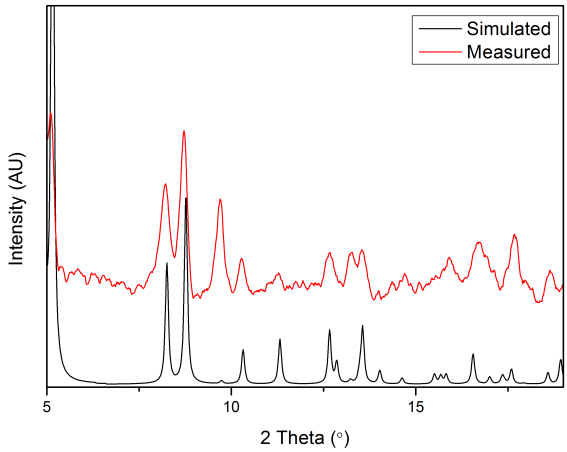

Figure S1: PXRD analysis of compound **TCM-9-Ho**, with the simulated pattern in black and the measured pattern in red.

4 Infrared Spectroscopy of TCM-9-Ho

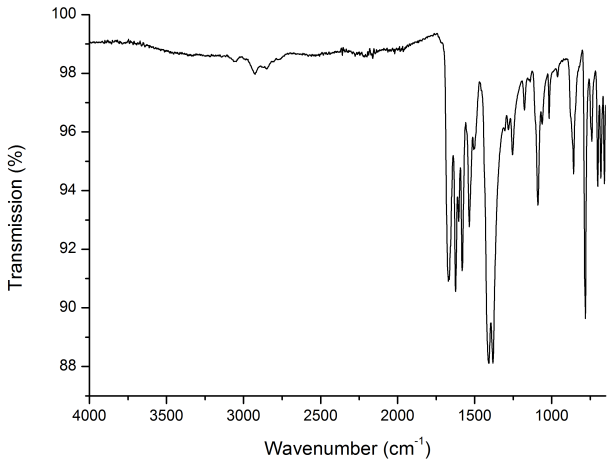

Figure S2: FT-IR spectrum of **TCM-9-Ho**.

5 Thermogravimetric Analysis of TCM-9-Ho

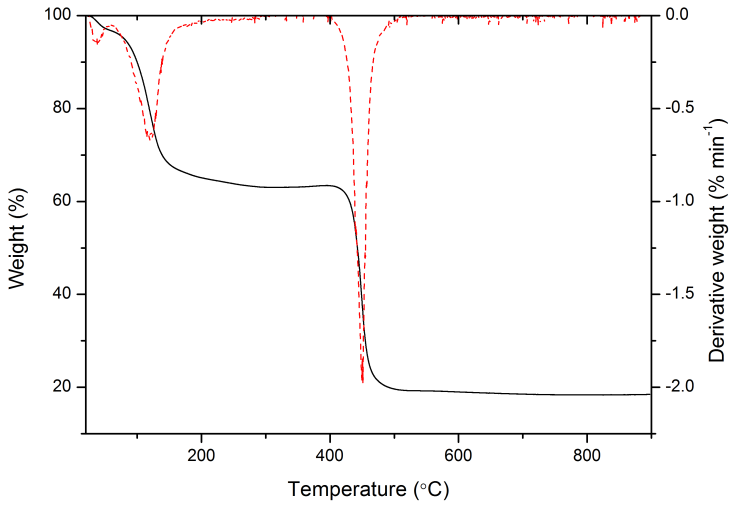

Figure S3: TGA of **TCM-9-Ho**.

6 Magnetic properties of TCM-9-Ho

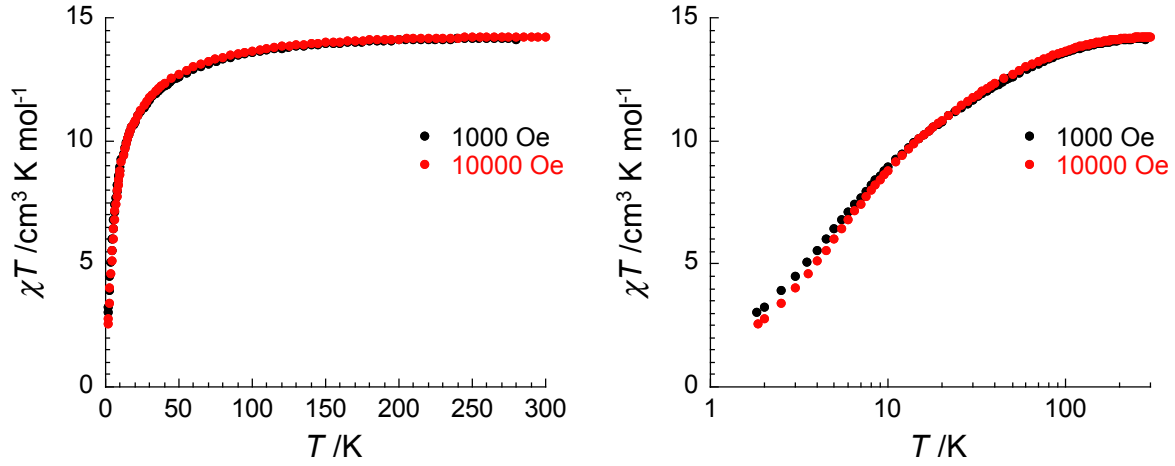

Figure S4: Temperature dependence of χT product at 1000 Oe (where χ is the molar magnetic susceptibility equal to the ratio between the magnetization and the applied magnetic field, *M/H*, per mole of Ho(III) complex) between 1.85 and 300 K for a polycrystalline sample of **TCM-9-Ho** in linear and semi-logarithm scales (left and right respectively).

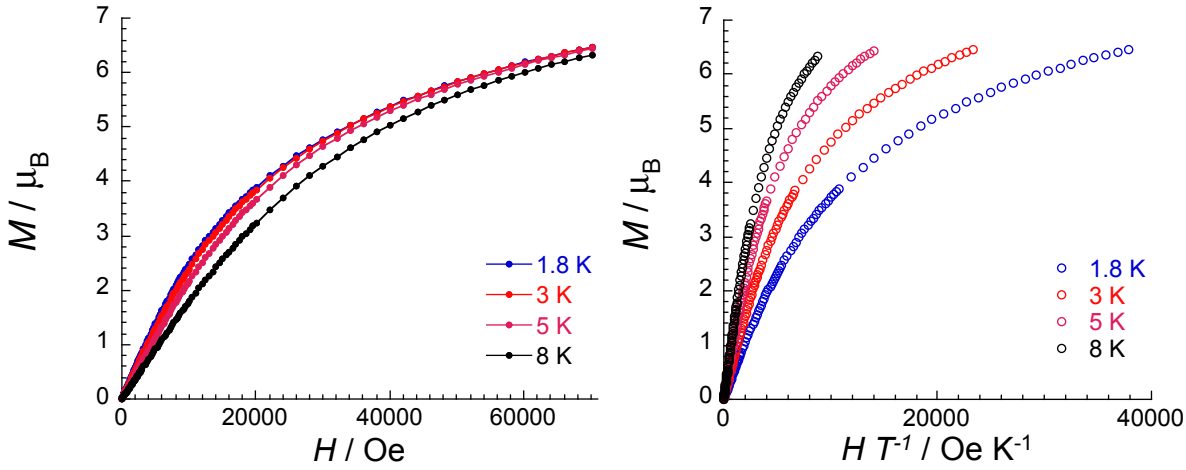

Figure S5: (Left) *M* vs *H* and (Right) *M* vs *H/T* for **TCM-9-Ho** between 1.85 and 8 K.

7 Magnetic properties of TCM-9-Dy

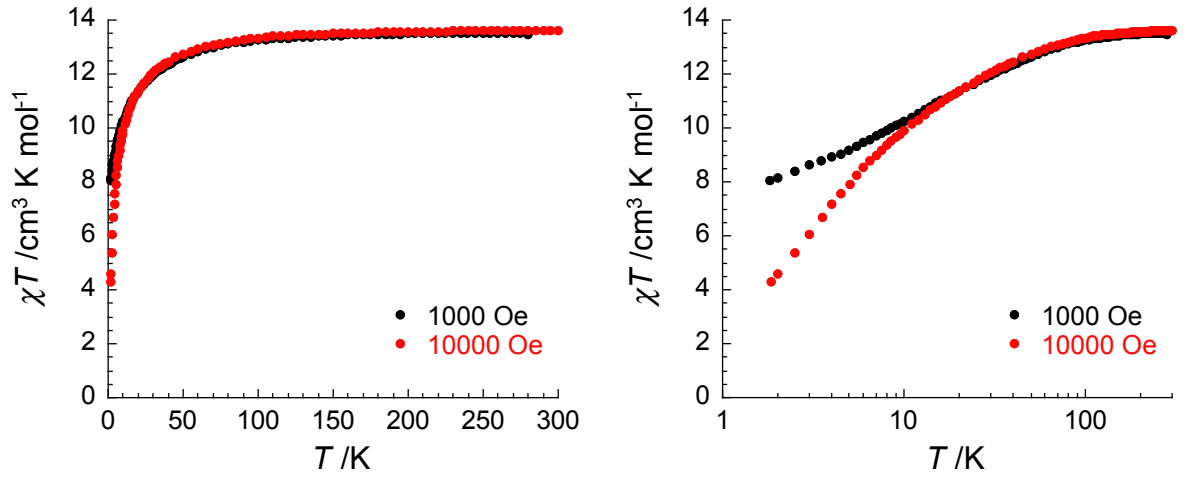

Figure S6: Temperature dependence of χT product at 1000 Oe (where χ is the molar magnetic susceptibility equal to the ratio between the magnetization and the applied magnetic field, M/H, per mole of Dy(III) complex) between 1.85 and 300 K for a polycrystalline sample of **TCM-9-Dy** in linear and semi-logarithm scales (left and right respectively).

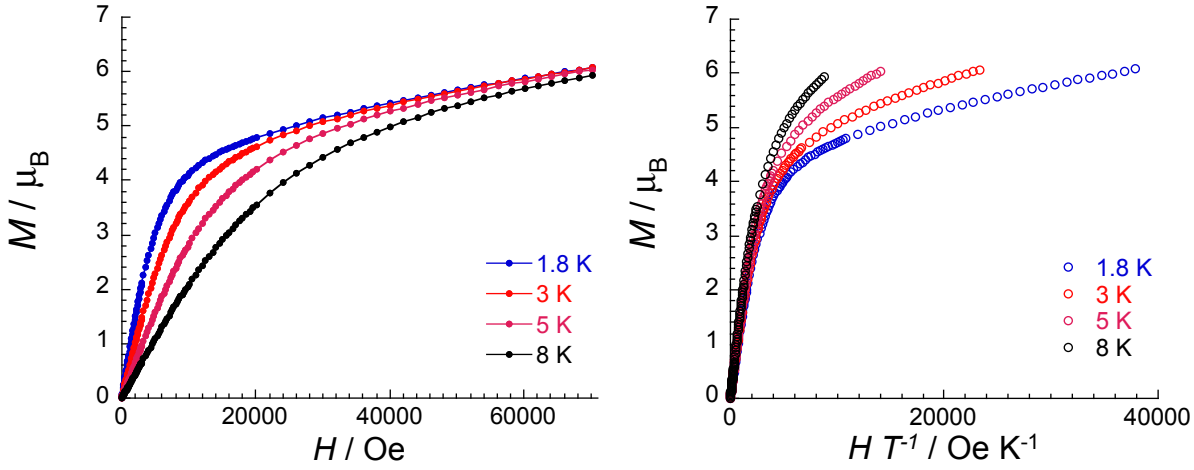

Figure S7: (Left) *M* vs *H* and (Right) *M* vs *H/T* for **TCM-9-Dy** between 1.85 and 8 K.

8 BET analyses and sample preparation of TCM-9-Ho

In order to determine the BET surface area of **TCM-9-Ho**, it was necessary to remove the DMF solvent molecules which reside in its pores/channels. Two methods were implemented to achieve this: removal of the DMF molecules using super critical CO_2 in a process known as critical point drying (CPD) or *via* solvent exchange using dichloromethane.

After the solvent exchange process using dichloromethane, the samples were transferred to an Autosorb-IQ volumetric analyser and subjected to surface area analysis after being heated under vacuum at 150 °C for 6 hours. Activation at lower temperatures does not seem to result in an open-framework structure that gives rise to permanent porosity. Upon heating to 150 °C the structure enabled the measurement of a stable surface area. The resulting amorphous solid has a broadly similar IR spectrum to that of the untreated sample, indicating that it has a comparable coordination environment, the differences may arise due to slightly different carboxylate coordination modes and the loss of coordination solvent molecules in the dried sample. The thermally treated material reveals a thermal degradation that is closely related to that of **TCM-9-Ho**. As for the pristine crystals, thermolysis of the organic ligand commences at *ca*. 400 °C providing further evidence of their related structures.

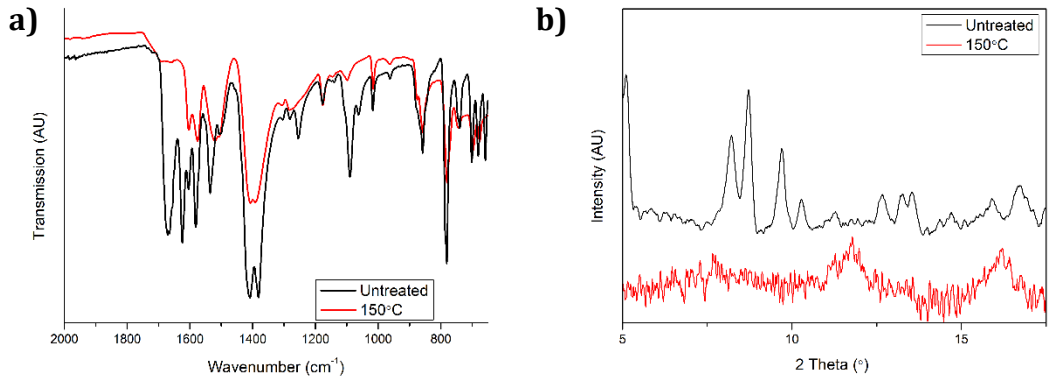

Figure S8: a) FT-IR and **b)** PXRD analysis, of an untreated sample of **TCM-9-Ho** and a sample heated under vacuum at 150 °C.

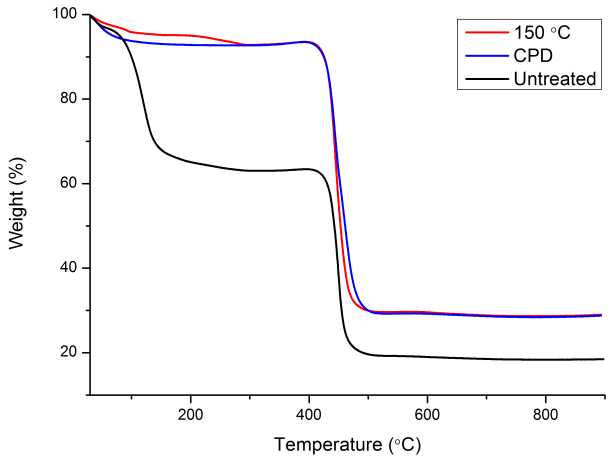

Figure S9: Comparison of the TGA curves of **TCM-9-Ho** and after desolvation at 150 °C and through CPD.

Critical point drying (CPD) using CO_2 super-critical CO_2 was used to replace the solvent molecules in **TCM-9-Ho**. The compound was first dispersed in dichloromethane and over a course of a few days the dichloromethane is exchanged with fresh solvent. After this procedure the material is placed in a high-pressure vessel, contained within a Quorum Technologies K850 Critical Point Drier and liquid CO_2 is transferred into the chamber which has been pre-cooled to 5 °C. The higher density of the dichloromethane causes it gradually to sink to the bottom of the chamber, at which point it can be removed through an opening at the base of the vessel. This process is repeated several times. At all times the sample is completely submerged in liquid CO_2 to ensure that dichloromethane does not directly evaporates. Once the dichloromethane has been removed, the chamber is slowly heated to 35-40 °C, resulting in an increase in pressure and the passing of the critical temperature and pressure points of CO_2. At this stage the meniscus of the liquid CO_2, which up until this point was visible through a glass window, disappears, due to the loss of surface tension and the CO_2 can be safely removed. An exhaust valve is opened and the CO_2 is very slowly released from the chamber. The sample can then be transferred to the Quantachrome Autosorb-IQ analyser for surface area measurements.

The gas sorption studies confirmed the permanent porosity of the thermally treated sample of **TCM-9-Ho**, with the two applied methods giving similar results. The solvent-exchange and CPD methods produced comparable type I N_2 isotherms, which demonstrate an initial steep increase, followed by a gradual rise in the uptake of N_2 without reaching saturation. The solvent exchange and CPD activation methods resulted in BET surface areas of *ca*. 765 $m^2 g^{-1}$ and 720 $m^2 g^{-1}$, respectively.

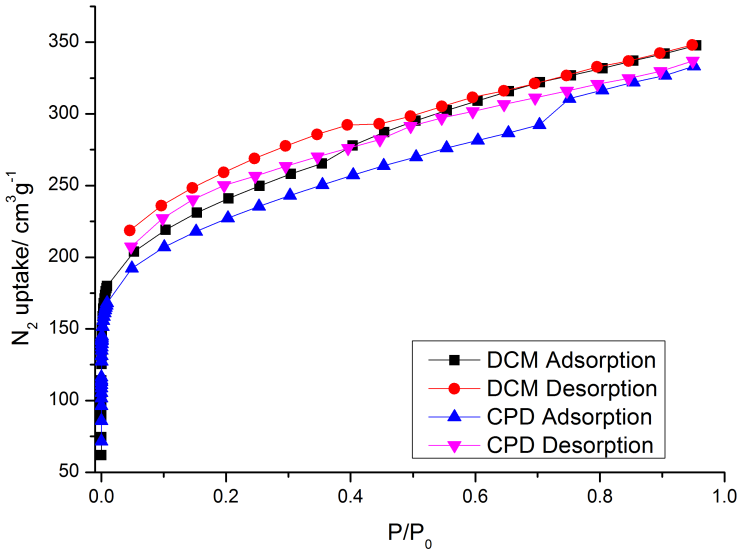

Figure S10: N_2 isotherms of **TCM-9-Ho**, after activation using dichloromethane and heating to 150 °C and through the CPD method.

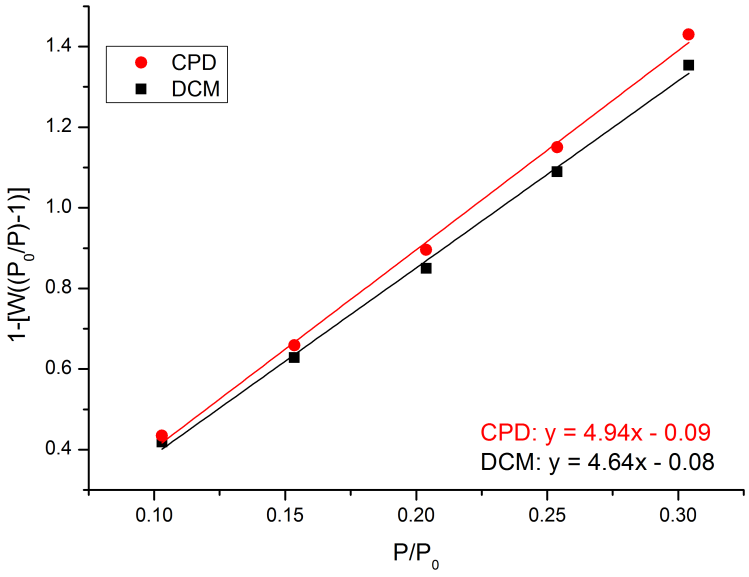

Figure S11: Plot of the linear region of the BET equation for **TCM-9-Ho** derived from the CPD (red) and dichloromethane (black) activated N_2 adsorption isotherms.

9 FT-IR spectra of related lanthanide MOFs (TCM-9-Ln)

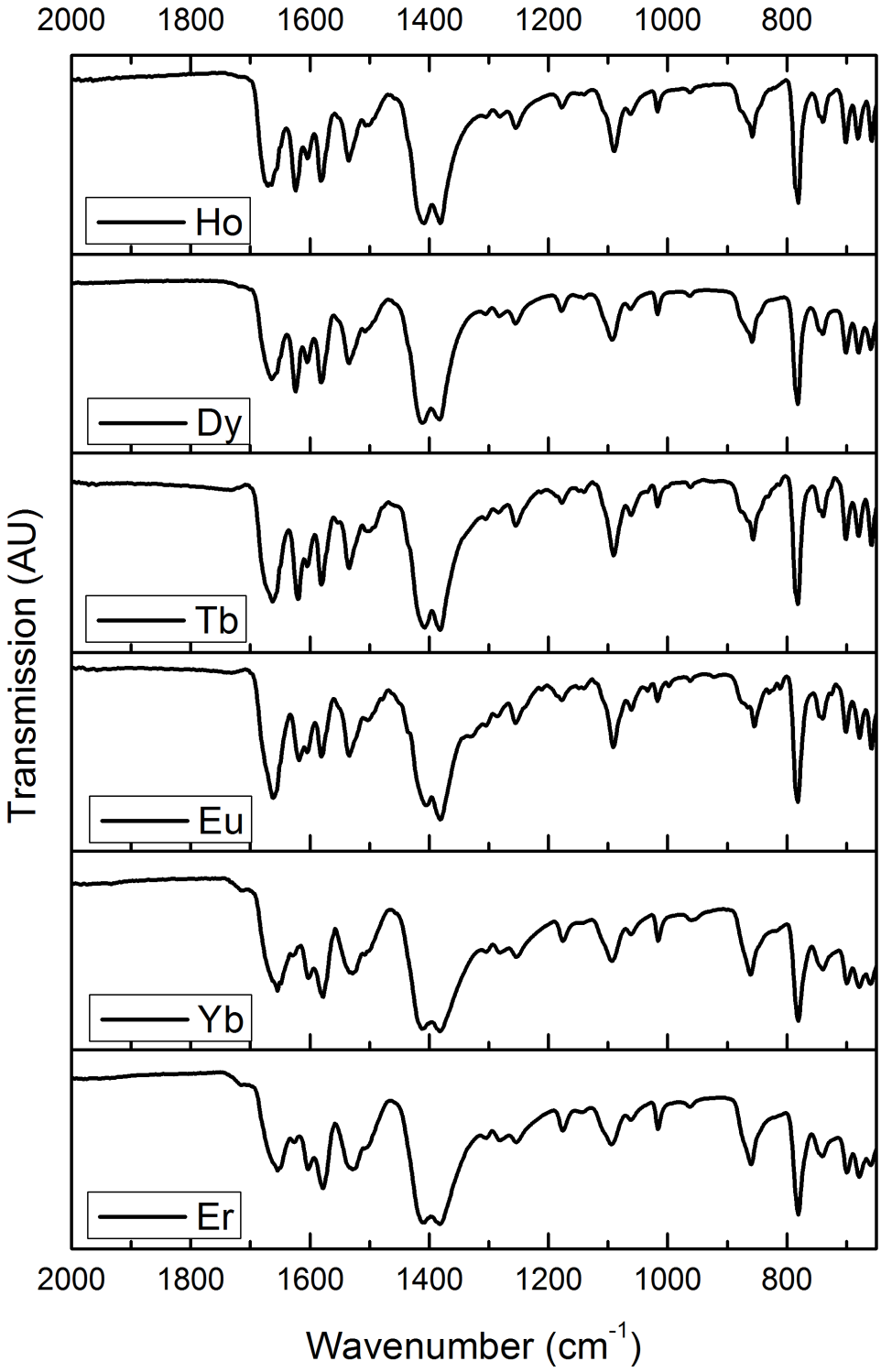

Figure S12: FT-IR spectra of the Dy^{III}, Tb^{III}, Eu^{III}, Yb^{III}, Er^{III} compounds structurally related to **TCM-9-Ho**.

.

10 Thermogravimetric analysis of MOFs (TCM-9-Ln)

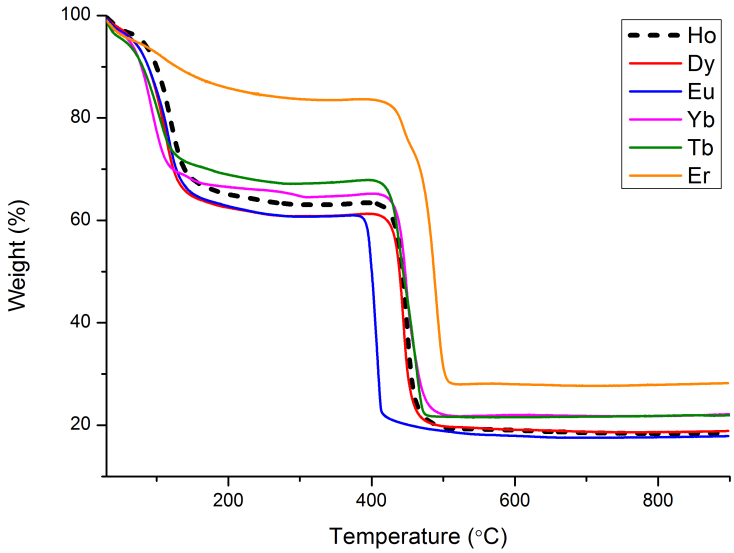

Figure S13: TGA of the lanthanide compounds structurally related to **TCM-9-Ho**.

11 PXRD studies of the Ln^{III} compounds structurally related to TCM-9-Ho

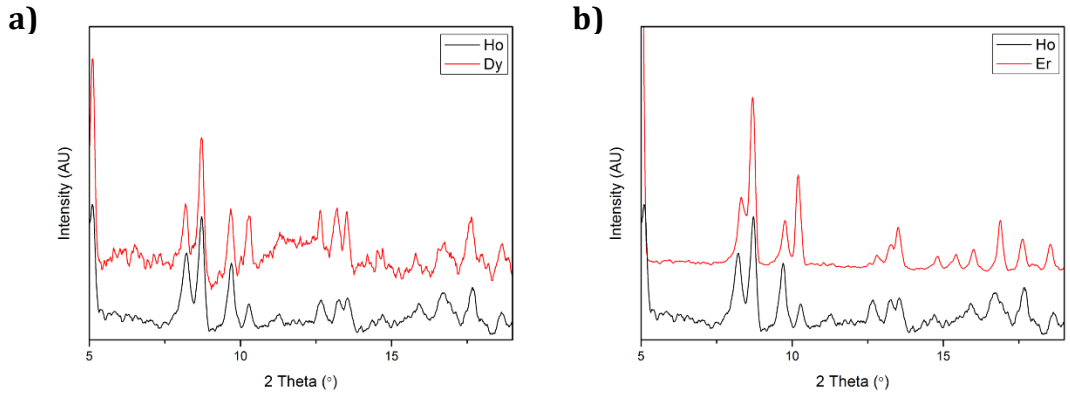

Figure S14: PXRD pattern of **a) TCM-9-Dy** and **b) TCM-9-Er** compared to **TCM-9-Ho**.

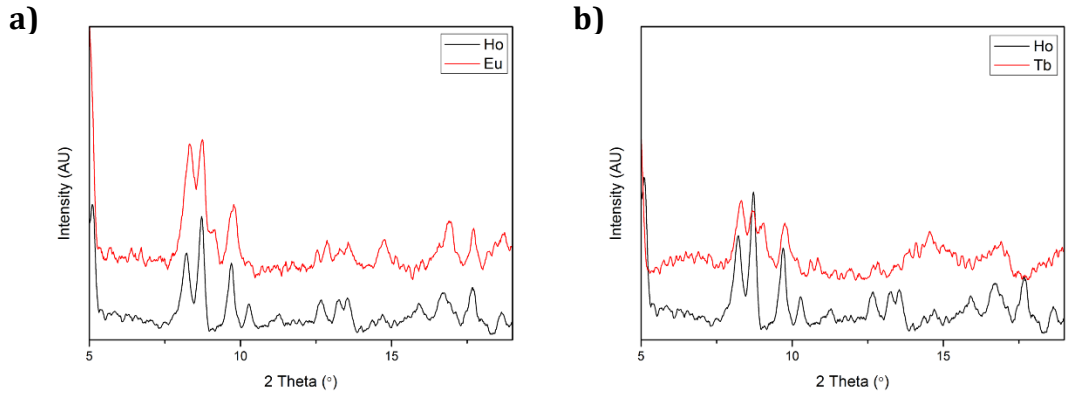

Figure S15: PXRD pattern of **a) TCM-9-Eu** and **b) TCM-9-Tb** compared to **TCM-9-Ho**.

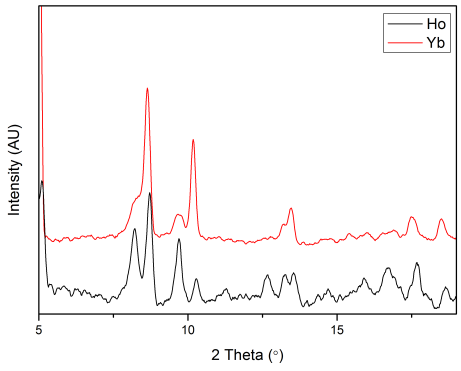

Figure S15: PXRD pattern of **TCM-9-Yb** compared to **TCM-9-Ho**.

12 Analysis of TCM-9-Nd

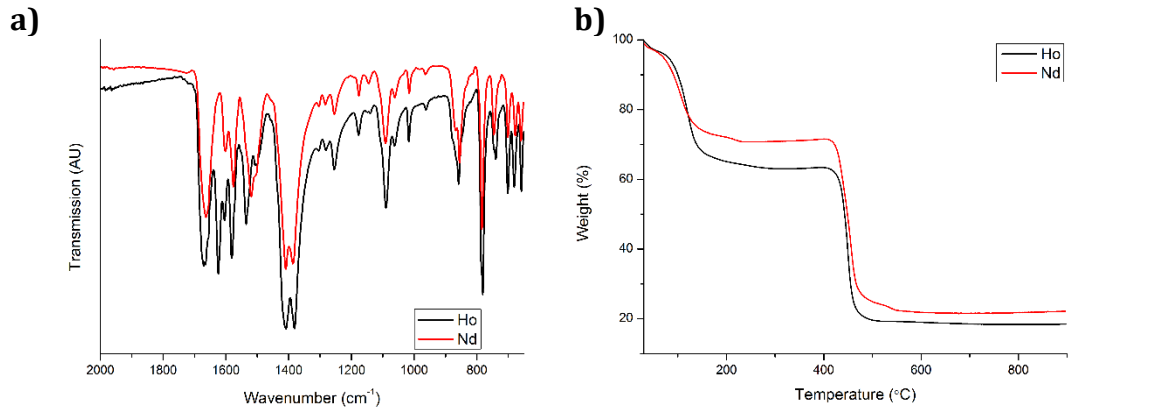

Figure S16: Comparison of the **a)** FT-IR spectra and **b)** TGA curves of **TCM-9-Ho** (black line) and **TCM-9-Nd** (red line).

13 Analysis of TCM-9-Sm

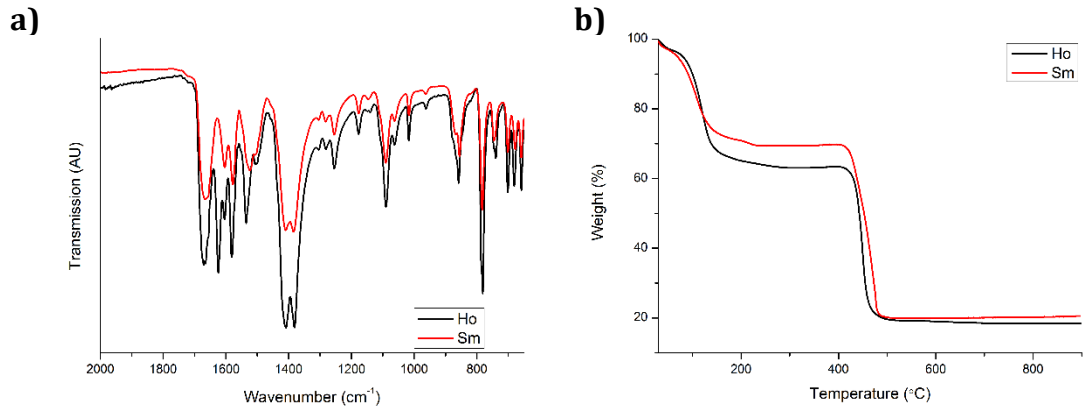

Figure Error! No text of specified style in document.**:** Comparison of the **a)** FT-IR spectra and **b)** TGA curves of **TCM-9-Ho** (black line) and **TCM-9-Sm** (red line).

14 Further spectroscopic characterization of the MOFs

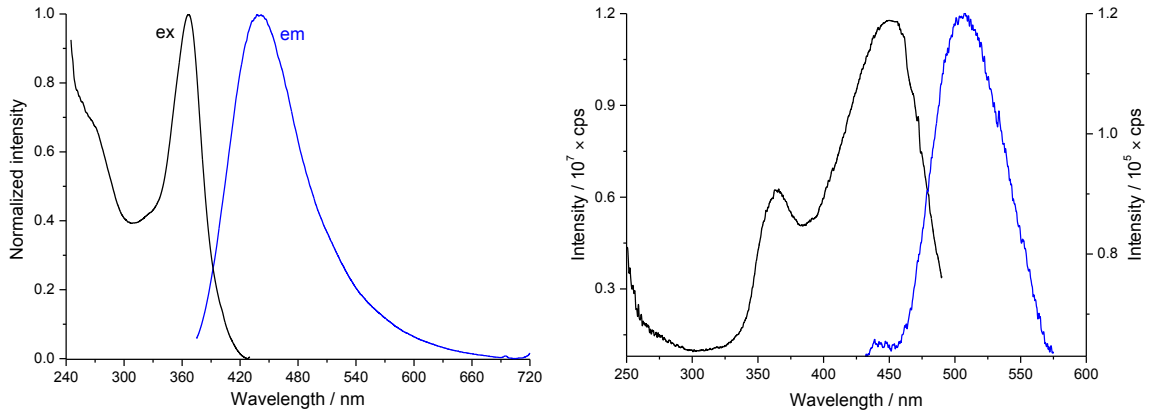

Figure S18: Ligand-centred emission and excitation spectra of **BTEB** (left; λ_{ex} = 365 nm, λ_{an} = 440 nm) and **TCM-9-Eu** (right; λ_{ex} = 365 nm, λ_{an} = 510 nm) in the solid state.

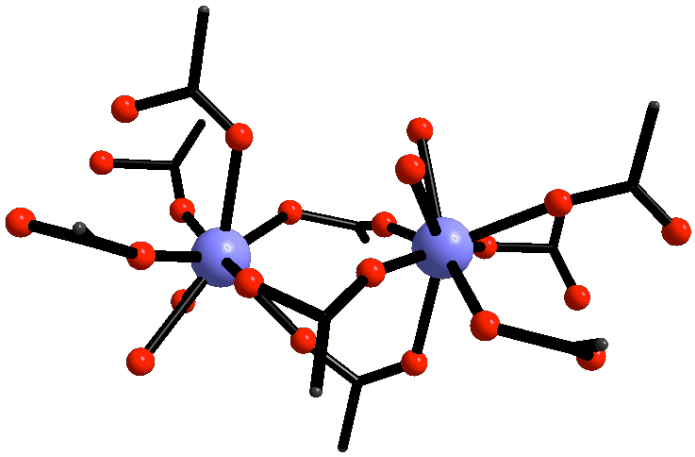

Figure S19: Coordination environment of the holmium ions in **TCM-9-Ho**.

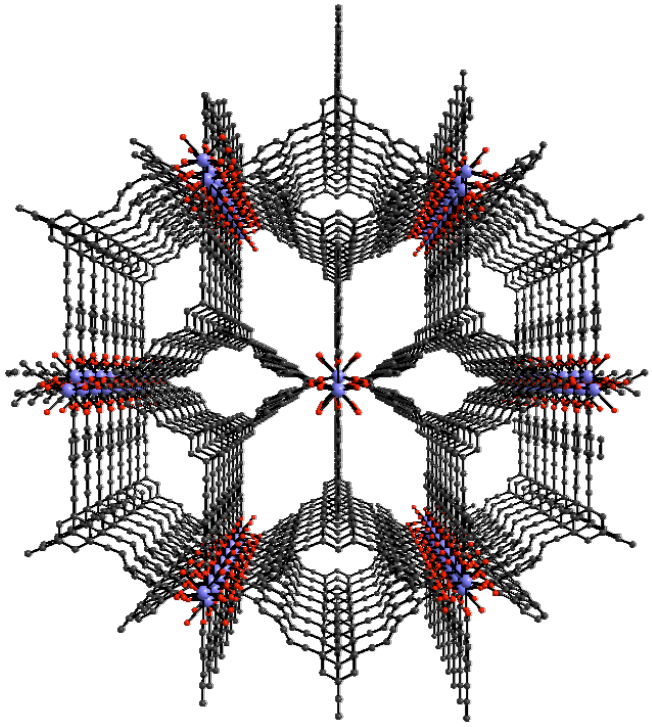

Figure S20: Structure of **TCM-9-Ho**.

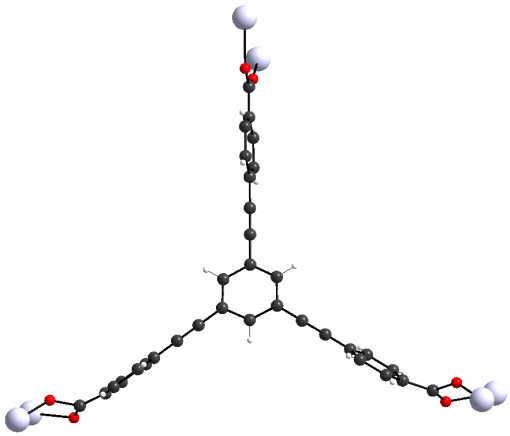

Figure S21: Image indicating the torsion angles between inner and outer phenyl rings of the BTEB ligand in **TCM-9-Ho**.

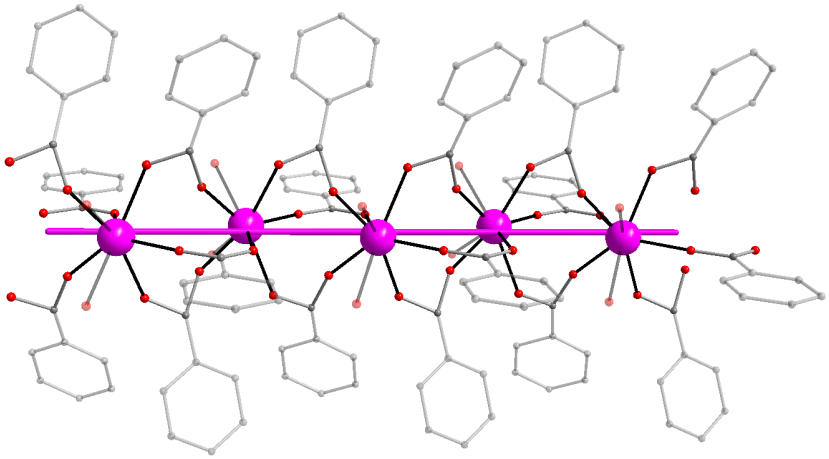

Figure S22: 1D-chain moiety in **TCM-9-Ho**.